JACS
JOURNAL OF THE AMERICAN CHEMICAL SOCIETY

Article

pubs.acs.org/JACS

Nanoelectrochemical Approach To Detecting Short-Lived Intermediates of Electrocatalytic Oxygen Reduction

Min Zhou, Yun Yu, Keke Hu, and Michael V. Mirkin*

Department of Chemistry and Biochemistry, Queens College, City University of New York, Flushing, New York 11367, United States

Supporting Information

ABSTRACT: Development of better catalysts for the oxygen reduction reaction (ORR) and other electrocatalytic processes requires detailed knowledge of reaction pathways and intermediate species. Here we report a new methodology for detecting charged reactive intermediates and its application to the mechanistic analysis of ORR. A nanopipette filled with an organic phase that is immiscible with the external aqueous solution was used as a tip in the scanning electrochemical microscope to detect and identify a short-lived superoxide ($O_2^{\bullet-}$) intermediate and to determine the rate of its generation at the catalytic Pt substrate and its lifetime in neutral aqueous solution. The voltammogram of the $O_2^{\bullet-}$ anion transfer to the organic phase provides a unique signature for unambiguous identification of superoxide. The extremely short attainable separation distance between the pipette tip and substrate surface (~1 nm) makes this technique suitable for detecting and identifying charged intermediates of catalytic processes with a lifetime of a few nanoseconds.

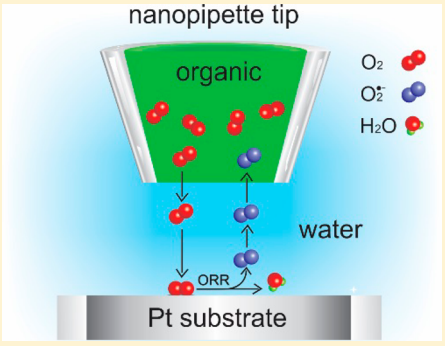

INTRODUCTION

The quest for efficient energy conversion and storage has resulted in significant research activity in the field of heterogeneous electrocatalysis.[1] Oxygen reduction reaction (ORR) is central to many technological systems (e.g., fuel cells and metal−air batteries) as well as biological processes and numerous diseases.[2−4] A large number of research publications during the last five decades focused on identifying efficient and economically viable catalysts for ORR and clarifying the details of its mechanism. Despite extensive efforts, basic questions about the ORR pathways and intermediate species involved in this process remain open. One controversial issue is the nature of the first step in the overall four-electron/four-proton ORR at Pt-based catalysts. Three possibilities considered in the literature include[5] (i) splitting of the O−O bond upon adsorption on two active sites, $O_2^* = O^* + O^*$; (ii) formation of the superoxide anion, $O_2^* + e^- = O_2^{-*}$; and (iii) proton-coupled electron transfer, $O_2^* + H^+ + e^- = HO_2^*$. One can differentiate between these pathways by detecting short-lived intermediate species involved in different steps. Adzic and co-workers reported decisive proof of superoxide intermediate ($O_2^{\bullet-}$) formation on a polycrystalline Pt surface in alkaline solutions.[5] In contrast, a detailed microkinetic model developed by the Nørskov group does not include this species as an ORR intermediate at the Pt(111) surface.[6] The higher complexity of ORR at Pt electrodes has recently been inferred from experiments in which a significant amount of hydroxyl ($OH^{\bullet}$) radical was produced in aqueous solution during the overall $4e^- + 4H^+$ electrochemical process.[7]

Adsorbed superoxide on catalytic surfaces has been observed using surface-sensitive spectroscopic techniques such as surface-enhanced infrared reflection absorption spectroscopy (SEIRAS)[5] or surface-enhanced Raman scattering (SERS).[8] However, detecting and identifying this species in aqueous solutions is difficult because of the short lifetime and the lack of a suitable spectroscopic technique. More stable ORR intermediates (e.g., hydrogen peroxide) have been measured in solution using rotating ring-disk electrodes,[9], interdigitated array electrodes,[10] or the scanning electrochemical microscope (SECM).[11−14] For short-lived intermediates, quantitative studies by fast electrochemical techniques are complicated by nonideal behavior due to the fouling, dissolution, and deactivation of the electrode surface.[13,15] Superoxide anion was detected electrochemically during ORR only in strongly alkaline aqueous solutions (i.e., 1 M KOH[16] or >6 M NaOH[17]), where this species is relatively stable. Differentiation between $O_2^{\bullet-}$ and other reactive oxygen species is also difficult because of the lack of selectivity, and the identification was based on the number of transferred electrons.[17]

Here we describe a new approach for the detection of short-lived charged intermediates based on electron transfer/ion transfer (ET/IT) mode of the SECM operation.[18] In an ET/IT SECM experiment (Figure 1), the tip is a nanometer-sized pipette filled with organic phase that is immiscible with the external aqueous solution. Oxygen is initially present only in the organic solution inside the pipette; during the

Received: December 8, 2014
Published: May 15, 2015

DOI: 10.1021/ja512482n
J. Am. Chem. Soc. 2015, 137, 6517−6523

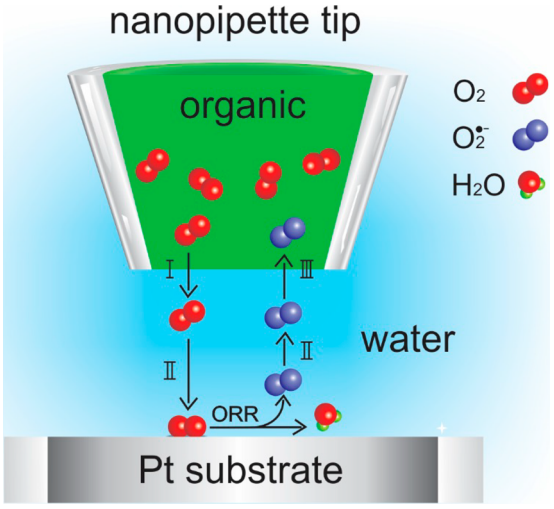

Figure 1. Schematic representation of the detection of superoxide intermediate ($O_2^{\bullet-}$) generated during ORR at the Pt substrate by ET/IT SECM technique: (I) oxygen partitioning from organic filling solution to the external aqueous phase; (II) diffusion; and (III) transfer of $O_2^{\bullet-}$ anion across the liquid/liquid nanointerface.

experiment, it partitions from organic to the aqueous phase. When the pipette is brought to within a few orifice radii of the catalytic Pt substrate, O_2 can diffuse to it and be reduced at the microscopic portion of the substrate surface facing the tip. A negatively charged ORR intermediate ($O_2^{\bullet-}$) can desorb from the Pt surface, diffuse to the pipette orifice, and be transferred into the filling organic solution by applying positive voltage between the reference electrode inside the pipette and the external reference. The resulting ion transfer (IT) current across the nanometer-sized liquid/liquid interface[19] is used to detect and identify the charged intermediate species—an important difference between the ET/IT SECM technique and previously reported applications of micrometer-sized pipettes to reagent delivery[20] and studies of electrocatalytic reactions.[21]

EXPERIMENTAL SECTION

Chemicals and Materials. Sulfuric acid (H_2SO_4, 99.999%), sodium sulfate (Na_2SO_4, ≥98%), sodium carbonate (Na_2CO_3, ≥98%), sodium hydroxide (NaOH, ≥97.0%, pellets), sodium hexafluorophosphate ($NaPF_6$, 98%), tetraethylammonium hydrogen sulfate ($TEAHSO_4$, 98%), 1-octanol (98%), methanol (98%), 1,2-dichloroethane (DCE, anhydrous, ≥99%), dimethyl sulfoxide (DMSO, BioReagent, for molecular biology, ≥99.9%), trimethylchlorosilane (TMSCl, 98%), bis(triphenylphosphoranylidene)-ammonium chloride (BACl), tetrabutylammonium perchlorate ($TBAClO_4$, ≥99%), and potassium tetrakis(4-chlorophenyl)borate (KTPBCl) were all from Sigma-Aldrich. All of these chemicals were used as received. Platinum wire (diameter, 25 μm) was from Goodfellow Company. Quartz capillaries were obtained from Sutter Instruments Co. (Novato, CA).

Bis(triphenylphosphoranylidene)ammonium tetrakis(4-chlorophenyl)borate (BATPBCl) and bis(triphenylphosphoranylidene)-ammonium hexafluorophosphate ($BAPF_6$) were prepared by metathesis of 1:1 mixtures of BACl and KTPBCl or $NaPF_6$ in methanol–water mixtures (v/v = 2:1) followed by recrystallization from acetone.[22] Anhydrous (≥99%) benzotrifluoride (BTF) from Sigma-Aldrich was purified by repeated boiling with aqueous Na_2CO_3 washing and then distilling under nitrogen at ambient pressure.[23] The thorough purification of BTF was essential for IT experiments because this reagent contained an unknown hydrophobic anionic species whose transfer wave appeared within the potential window. The purification protocol was repeated until no impurity transfer wave could be detected in background IT voltammograms.

To prepare a Ag/AgTPBCl reference,[24] the compact layer of AgTPBCl was slowly deposited onto a precleaned Ag wire by constant-current electrolysis in 0.01 mM KTPBCl methanol/water (1:1) solution.

Nanopipettes and Electrodes. The nanopipettes were fabricated from quartz capillaries using a laser-based pipette puller (P-2000, Sutter Instrument Co.), as described previously.[18,25] A suitable program was selected to pull pipettes with the short inner shaft, thus minimizing the internal resistance. Different procedures were used to prepare pipettes for filling with either aqueous or organic solution. In the former case, to render the outer wall hydrophobic, the pipette was held approximately 1 cm above liquid TMSCl for about 2 min while the flow of argon was passed through its back to avoid silanization of the inner wall.[26] For organic-filled pipettes, the silanization was performed using a slightly modified version[18] of the previously described procedure.[27] Briefly, the nanopipette was fixed in a glass vacuum desiccator (Fisher-Scientific), which was connected to a thermocouple gauge controller (KJLC 205 series, Kurt J. Lesker Co.) and a pump (RV8, Edwards Co.). The desiccator was first evacuated by the pump, and then the TMSCl vapor was delivered from the flask to the desiccator, where the nanopipette was exposed to it for about 45 min. The system was evacuated again to remove the silane vapor before the pipettes were taken out.

The current–distance curves were obtained with a glass-sealed 25 μm diameter Pt disk electrode polished on the 50 nm alumina and used as a substrate. Its surface roughness of <5 nm over the 1 μm × 1 μm area, as evaluated from noncontact mode atomic force microscopy images,[28] was small in comparison with the radii of the pipette tips employed in this study (a > 60 nm). Before use, the Pt substrate was electrochemically cleaned in 0.5 M H_2SO_4 aqueous solution. The substrate potential was either controlled with respect to the external reference electrode or allowed to float at open circuit (unbiased substrate).

Instrumentation and Procedures. SECM experiments were carried out using a home-built instrument.[18] To obtain an SECM approach curve, the nanopipette tip was first positioned a few hundred micrometers above the Pt substrate using positioning stages. To avoid crashing, this process was monitored with a long-distance video microscope. Then, the nanopipette tip was moved closer to the substrate in the automated "surface hunter" mode until the IT current decreased by about 10%. Both the substrate and tip currents were collected during the subsequent fine approach. The same instrument was used to record tip and substrate voltammograms. The oxygen delivery experiments were performed in a homemade electrochemical cell after the aqueous solution was purged with argon.

Selection of Organic Solvent and Electrolyte. An ORR intermediate—superoxide—is an anionic radical known to react with many organic substances.[29] The selection of organic solvent and electrolyte inert toward this highly reactive species was critical for the present study. The reversible one-electron ORR in aprotic DMSO (Figure 2a) was used to check the stability of specific solvent and electrolyte toward the electrogenerated $O_2^{\bullet-}$.[30] For instance, DCE—a solvent commonly used in liquid/liquid electrochemistry—is expected to be oxygenated by superoxide.[31] When DCE was added to DMSO, its reaction with electrogenerated $O_2^{\bullet-}$ resulted in the disappearance of the anodic peak, while the cathodic peak was markedly enhanced (Figure 2b) due to the regeneration of O_2 via rapid nucleophilic and electron transfer reactions of $O_2^{\bullet-}$.[30,31] In contrast, the addition of chemically inert BTF[32] to DMSO had no effect on the ORR voltammogram (Figure 2c). Similarly, BATPBCl can be employed as an electrolyte because its anion, $TPBCl^-$, cannot be oxygenated by $O_2^{\bullet-}$ despite being a halogenated aromatic hydrocarbon.[31] The reversible ORR wave in Figure 2d points to the BATPBCl stability in the presence of $O_2^{\bullet-}$.

Electrochemical Cells. SECM experiments were carried out in a three-electrode cell that included the Pt substrate and two reference

DOI: 10.1021/ja512482n
J. Am. Chem. Soc. 2015, 137, 6517–6523

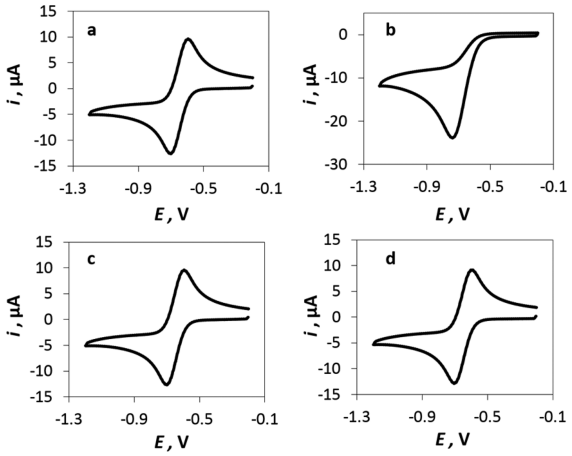

Figure 2. Checking stability of solvent and electrolyte by ORR voltammetry. (a) DMSO solution only contained 100 mM $TBAClO_4$. The same solution also contained 5 mM of either DCE (b), BTF (c), or BATPBCl (d). Voltammograms were obtained in a three-electrode cell with a 3 mm diameter working glassy carbon electrode, a 0.5 mm diameter Ag wire quasi-reference, and a 2 mm diameter Pt wire counter electrode. Scan rate was 100 mV/s.

electrodes placed inside the pipette and in the outer solution. Both the substrate and tip potentials were measured versus the outer reference electrode. Ion transfer current to the pipette filled with either organic or aqueous solution was measured in Cell 1 or Cell 2, respectively.

$$\underset{\text{outer aqueous solution}}{\text{Ag | AgCl | 100 mM } Na_2SO_4,\ 0.5 \text{ mM } TEA_2SO_4} \parallel \underset{\text{BTF in pipette}}{\text{100 mM BATPBCl| AgTPBCl | Ag}} \quad \text{(Cell 1)}$$

$$\underset{\text{outer BTF solution}}{\text{Ag | AgTPBCl | 100 mM BATPBCl, 0.75 mM } BAPF_6} \parallel \underset{\text{aqueous phase in pipette}}{\text{100 mM } Na_2SO_4\text{| AgCl | Ag}} \quad \text{(Cell 2)}$$

RESULTS

Figure 3 shows the controlled delivery of oxygen from the pipette filled with BTF solution to the 25 μm diameter

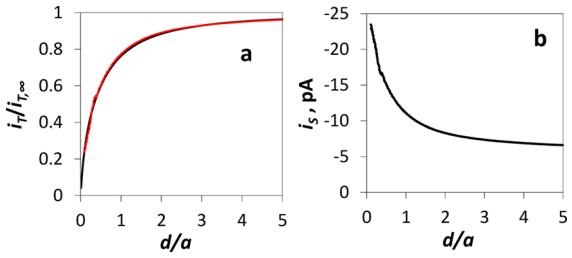

Figure 3. Oxygen delivery from the BTF-filled pipette used as an SECM tip to the Pt substrate. Experimental current−distance curve based on the TEA^+ transfer from the external aqueous phase to the organic filling solution (red line; Cell 1) fitted to the theory (black line[33]) for the SECM negative feedback (a) and corresponding i_S vs d/a dependence for the reduction of oxygen delivered from the pipette (b). E_T = −0.4 V, E_S = −0.5 V. $i_{T,\infty}$ = −97.8 pA is the i_T value in the bulk solution. The pipette orifice radius, a = 225 nm; the Pt substrate diameter was 25 μm.

polycrystalline Pt substrate immersed in aqueous solution. The pipette geometry was characterized by steady-state voltammetry and TEM (Supporting Information (SI), Figure S1). The tip current (i_T) in Figure 3a is due to the transfer of a tetraethylammonium (TEA^+) cation from the external aqueous solution to the pipette, which was driven by the negative voltage (E_T = −0.4 V) applied between the internal and external reference electrodes. This voltage corresponds to the diffusion-limiting current of TEA^+ transfer (SI, Figure S1), while Na^+ transfer did not occur because its onset potential is about −0.6 V. The tip current decreased with the decreasing tip/substrate separation distance (d) because the Pt substrate blocked the diffusion of TEA^+ to the orifice (Figure 3a; negative feedback). By fitting the experimental current−distance curve (red line) to the theory (black line),[33] we could determine and control the separation distance. The substrate current (i_S) produced by ORR increased with decreasing d (Figure 3b), as expected from the previously developed theory.[18]

We used the transfer of the superoxide anion across the BTF/water nanointerface for the detection and identification of this species. To our knowledge, the IT of superoxide has not yet been studied, and the standard ion transfer potential[19] value required for identifying $O_2^{\bullet-}$ is not known. Unlike aqueous solutions, the superoxide anion is stable in aprotic solvents, in which it is readily produced via the one-electron ORR.[30] Reversible cyclic voltammograms of this process were obtained at the millimeter-sized glassy carbon electrode in BTF solution (Figure 4a). The same process produced steady-

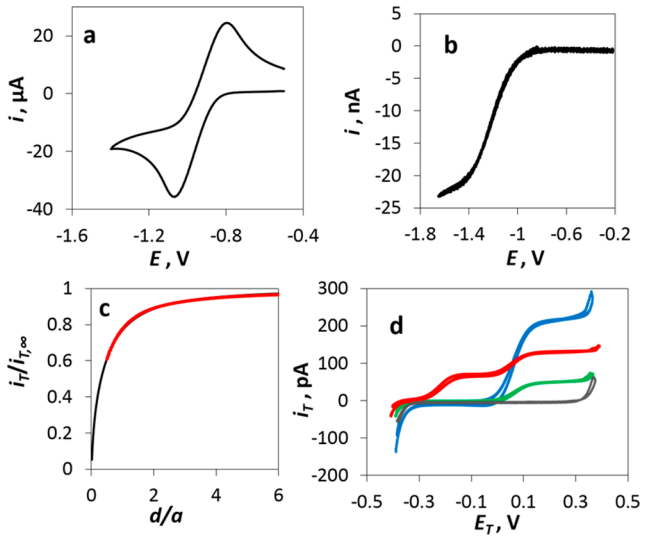

Figure 4. Superoxide anion generation in BTF and collection at the water-filled pipette tip. Voltammograms of ORR obtained at the 3 mm diameter glassy carbon electrode (a) and 25 μm diameter Pt SECM substrate (b) in BTF solution containing 100 mM BATPBCl. The reference electrode was Ag/AgTPBCl. (c) Experimental current−distance curve obtained with a nanopipette tip (a = 252 nm) approaching an unbiased Pt substrate (red line) fitted to the theory for the negative feedback (black line). E_T = 0.3 V. (d) IT voltammograms obtained at the same pipette and d = ∞ (blue) and 125 nm (red and green). Pt substrate was unbiased except for the red curve, where E_S = −0.9 V. In (c) and (d), the experiments were performed in Cell 2. The background curve (black curve in d) was obtained with no $BAPF_6$ in BTF.

state voltammograms at the Pt microelectrode (Figure 4b). To measure the IT of $O_2^{\bullet-}$, a pipette tip was filled with aqueous solution and brought within the limits of the diffusion layer generated at the Pt substrate in BTF solution. The application of a positive potential to the pipette tip induced the ingress transfer of PF_6^- from the external BTF solution (blue curve in Figure 4d). This current decreased

DOI: 10.1021/ja512482n
J. Am. Chem. Soc. 2015, 137, 6517−6523

with the decreasing distance between the pipette orifice and the unbiased Pt substrate, and the resulting experimental approach curve (red line in Figure 4c) fits the theory for the negative feedback well (black line in Figure 4c[33]).

The same effect can be seen in IT voltammograms: the diffusion-limiting current of the PF_6^- transfer in the bulk solution (blue curve in Figure 4d) was much higher than that in the voltammogram obtained at the same pipette and d = 125 nm (green curve). When the Pt substrate potential was −0.9 V, the new anion transfer wave with the half-wave potential, $E_{1/2}$ = −0.25 V, appeared in the IT voltammogram (red curve in Figure 4d), which was obtained at the same d = 125 nm as the green curve. E_S = −0.9 V corresponds to the foot of the ORR wave in Figure 4b. At more negative substrate potentials, the tip current became very high because of the high solubility of O_2 in BTF solution, and thus, a large amount of superoxide anion was generated at the substrate.

A 53 nm radius BTF-filled pipette was used to detect the superoxide intermediate produced during ORR at the Pt substrate in neutral aqueous solution (Figure 5). The

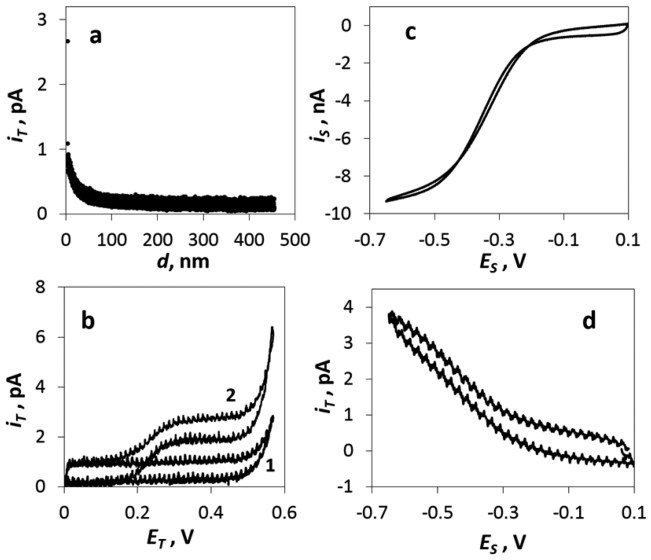

Figure 5. Detection of superoxide intermediate produced during the ORR in aqueous solution. (a) Current−distance curve obtained with a BTF-filled 53 nm radius pipette approaching the Pt substrate. E_T = 0.4 V and E_S = −0.5 V. (b) IT voltammograms obtained with the same pipette at d = 100 (1) and 40 (2) nm; E_S = −0.5 V. ORR voltammogram at the substrate (c) and corresponding i_T vs E_S dependence (d) obtained at E_T = 0.4 V and d = 40 nm. (a−d) Experiments were carried out in Cell 1.

current−distance curve in Figure 5a was obtained with the E_S = −0.5 V vs Ag/AgCl reference, at which ORR occurred at the substrate (Figure 5c). E_T = 0.4 V corresponded to the plateau of the superoxide anion transfer across the BTF/water nanointerface [in this experiment, $E_{1/2}$ = +0.25 V for $O_2^{\bullet-}$ transfer in Cell 1 as opposed to −0.25 V in Figure 4d because, in the latter case, the filling solution was aqueous and the outer solution was BTF (Cell 2)], and no other ionic species could be transferred at this potential (the polarization window is shown in SI, Figure S7). The i_T in Figure 5a was negligibly small at longer separation distances and increased sharply at $d \leq$ ~50 nm. The current−distance curve obtained under the same experimental conditions using a much larger pipette (a = 110 nm; Figure S2 in SI) also showed that the i_T increases over the d range of ~50 nm. Moreover, no waves can be seen in the tip voltammogram obtained at d = 100 nm (curve 1 in Figure 5b), and a well-defined anion transfer wave appears at d = 40 nm (curve 2 in Figure 5b). There is also close correspondence between the voltammogram of the ORR at the Pt substrate (Figure 5c) and the IT wave in the i_T versus E_S dependence obtained at d = 40 nm (Figure 5d).

The complete ET/IT SECM experiment, including the delivery of O_2 from the nanopipette tip, its reduction at the Pt catalytic substrate, and the collection of $O_2^{\bullet-}$ at the BTF/water nanointerface, is presented in Figure 6. The substrate potential was −0.5 V vs Ag/AgCl reference, corresponding to the plateau region in the ORR voltammogram (Figure 5c), and the tip potential of 0.4 V was sufficiently positive for the diffusion-limiting IT of $O_2^{\bullet-}$. The same set of parameters was used to fit the i_S versus d (Figure 6a) and i_T versuss d (Figure 6b) curves obtained with the same 69 nm radius pipette. The i_S versus d theoretical curve was calculated using the previously developed model[18] (simulation package COMSOL Multiphysics version 4.4 was employed; see SI for details), while the tip response was simulated assuming the decomposition of $O_2^{\bullet-}$ via a pseudo-first-order reaction in neutral aqueous solution.

DISCUSSION

The partitioning of a neutral oxygen molecule from the pipette to the external aqueous solution is not affected by the interfacial potential and does not contribute to the tip current. Thus, some interfacial IT process unrelated to ORR is needed to control the tip/substrate separation distance. In Figure 3a, TEA^+ transfer was used to measure d via negative SECM feedback and bring the pipette tip within a ~0.5a distance from the Pt substrate. The substrate current (Figure 3b) is due to the reduction of oxygen delivered from the pipette (the aqueous solution was degassed before the experiment). The 12.5 μm radius of the Pt substrate was sufficiently small to enable quantitative measurements of the pA-range ORR current and, at the same time, much larger than a to ensure high collection efficiency of the delivered oxygen (>90% for the entire distance range in Figure 3b[18]). The diffusion-limiting flux of O_2 from the pipette to the external solution is[18]

$$J_{max} = 4f(\theta)Dc^*a \quad (1)$$

where $f(\theta)$ is a factor related to the pipette angle θ,[34] c^* is the bulk concentration, and D is the diffusion coefficient of O_2 in BTF solution. Equation 1 represents the maximum flux value, corresponding to the complete partitioning of O_2 molecules from BTF to water. The flux of oxygen actually delivered from the pipette to the external solution depends on its partition coefficient K (i.e., the ratio of equilibrium concentrations of oxygen in BTF and water). This flux increases with decreasing d because the depletion of the oxygen concentration by ORR at the substrate shifts the partitioning equilibrium.[18] This effect resulted in the increase in i_S with decreasing d in Figure 3b. The comparison of the experimental i_S versus d dependence to the theory in ref 18 suggests that K > 10.

The half-wave potential of the IT across the BTF/water nanointerface can be used as a unique signature for unambiguous identification of $O_2^{\bullet-}$ species. A reversible cyclic voltammogram (Figure 4a) similar to the one-electron

DOI: 10.1021/ja512482n
J. Am. Chem. Soc. 2015, 137, 6517−6523

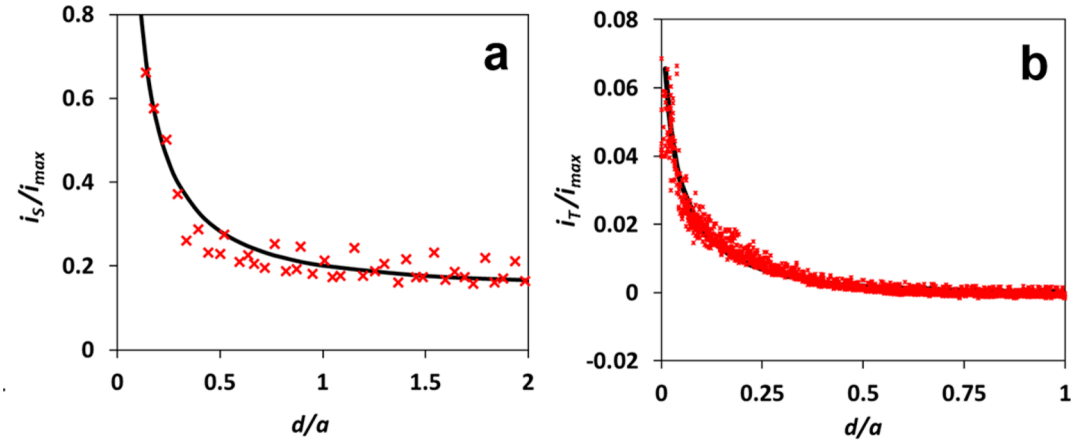

Figure 6. Experimental (symbols) and theoretical (solid lines) current−distance curves for oxygen delivery from the nanopipette to the Pt substrate and collection of the superoxide intermediate. The tip was a 69 nm radius pipette containing BTF solution (Cell 1) saturated with O_2, and the substrate was a 25 μm diameter Pt disk. Both the substrate (a) and tip (b) currents are normalized by the diffusion-limiting flux of oxygen from the nanopipette ($i_{max} = FJ_{max}$; eq 1[18]). E_T = 0.4 V and E_S = −0.5 V. The approach speed was 50 nm/s (a) and 1 nm/s (b).

ORR responses obtained previously in aprotic solvents[35] confirms the formation and stability of the superoxide anion in BTF solution containing BATPBCl electrolyte. The correct choice of suitable organic solvent and electrolyte is critical because superoxide can react with many of them either as a reducing agent or as an oxidant or a nucleophile.[29] In addition to the stability of BTF, the high oxygen solubility[32] and wide potential window[22] were advantageous for our experiments.

The IT wave with the $E_{1/2}$ = +0.05 V (blue, green, and red curves in Figure 4d) was obtained in Cell 2 for the transfer of PF_6^- from BTF to water at any d and E_S. In contrast, the IT wave with the $E_{1/2}$ = −0.25 V was observed only when the pipette tip was brought within a short distance from the Pt substrate, and the E_S was sufficiently negative for ORR in BTF solution (red curve in Figure 4d). This wave is due to the transfer of an anionic product of ORR, which in aprotic BTF solvent can only be $O_2^{\bullet-}$ species.

In experiments represented in Figure 5, the BTF-filled pipette was immersed in the external aqueous solution (Cell 1), and the supporting electrolytes in both liquid phases were the same as those in Cell 2. Thus, the half-wave potential of +0.25 V measured for the IT of an ORR intermediate (curve 2 in Figure 5b) corresponds to the $E_{1/2}$ = −0.25 V found for the $O_2^{\bullet-}$ transfer from BTF to water (red curve in Figure 4d). Considering possible ORR intermediates and products in aqueous solution, one can unambiguously attribute the IT wave in Figure 5b to the $O_2^{\bullet-}$ transfer. Indeed, the transferred species has to be anionic (the neutral molecules, such as H_2O_2, cannot contribute to the IT current, and the transfer of a cation would result in the current flowing in the opposite direction). The transfer of strongly hydrophilic OH^- occurs outside the polarization window. The only known anionic intermediate of the ORR in aqueous solution besides superoxide is HO_2^-. The possibility of this species being formed at the neutral pH and having sufficiently long lifetime to contribute to the IT current is remote because of the small acid ionization constant of H_2O_2 (pK_a = 11.6[36]). Figure S3 (SI) shows that the voltammetric wave of IT of an anionic ORR product from BTF to water completely disappeared after 2.5 mM of 1-octanol was added to the organic phase. $O_2^{\bullet-}$ is known to react with 1-octanol in aprotic solvents, producing HO_2^-.[30] From Figure S3 in the SI, one can conclude that the transfer wave of hydrophilic HO_2^- is outside the polarization window, and therefore, the wave in Figure 5b can only be due to the $O_2^{\bullet-}$ anion transfer. The possibility to selectively identify a short-lived intermediate based on its charge and IT potential is a major advantage of the developed approach.

A salient feature in the i_S versus d curve (Figure 5a) is that the tip current is measurable only at very short separation distances ($d \leq$ ~50 nm). In a substrate generation/tip collection SECM experiment, the distance scale is determined by the substrate radius. If the anionic species generated at the substrate in Figure 5a were stable, the i_T increase would have been observed over the d range of >12.5 μm. The distance scale in Figure 5a, which is several orders of magnitude smaller, is determined by the lifetime of substrate-generated superoxide radical. From Figure 5a,b, the maximum thickness of the tip/substrate gap that $O_2^{\bullet-}$ can cross during its lifetime is ~50 nm. As expected, this distance is independent of the pipette radius. In the i_T versus d curve obtained with a much larger pipette tip (a = 110 nm, Figure S2 in SI), the longest d at which the tip current value was measurable is also ~50 nm. Combining the diffusion distance of 50 nm with the diffusion layer thickness expressed as $2(Dt)^{1/2}$ [37] and $D = 6.7 \times 10^{-6}$ cm^2/s[38] yields a rough estimate for the time scale of $O_2^{\bullet-}$ decomposition in neutral aqueous solution on the order of 1 μs.

Because the substrate radius is much larger than a, the collection efficiency in substrate generation/tip collection experiments (i_T/i_S) is very small (<1%; cf. currents in Figures 4b and 4d), impairing quantitative analysis of the current−distance curves. The analysis of the ET/IT mode SECM experiment involved simulating the current distance curves for both substrate (Figure 6a) and tip (Figure 6b) processes (see SI for simulation details). The substrate response reflects the delivery of oxygen from the nanopipette and its reduction at the Pt surface. The shape of the simulated curve in Figure 6a is determined by several parameters, such as the diffusion flux of O_2 to the pipette orifice (J_{max} defined by eq 1), its partition coefficient (K), the ratio of the diffusion coefficients of O_2 in water and BTF, and the effective number of electrons transferred in the ORR (n). The i_{max} = 106 pA and the D_{O_2} (water)/D_{O_2} (BTF) = 0.57 were determined independently

DOI: 10.1021/ja512482n
J. Am. Chem. Soc. 2015, 137, 6517−6523

and not used as adjustable parameters.[39] The K value largely determines the curvature of the substrate current−distance dependence,[18] while the i_S magnitude at any d is directly proportional to n. Thus, both K = 145 and n = 3.6 could be confidently found from the best fit in Figure 6a. The latter value is consistent with the prevalence of $4e^-$ ORR to water with relatively small production of desorbed intermediates.[7,14]

The same values of K, J_{max}, and D_{O_2} (water)/D_{O_2} (BTF) parameters were used to fit both current−distance curves in Figure 6a,b. The tip current also depends on the rates of $O_2^{\bullet-}$ production at the substrate, its diffusion, and decomposition in water. These parameters can be determined from the best fit to simulated curves (Figures S5 and S6 in SI). The first quantity can be expressed as the diffusion flux of O_2 to the substrate multiplied by the empirical factor γ, where γ is the number of moles of $O_2^{\bullet-}$ desorbing from the Pt surface normalized by the total number of moles of reduced oxygen. The γ = 0.09 obtained from the best fit in Figure 6b is consistent with a relatively small fraction of ORR intermediates being desorbed to aqueous solution (n = 3.6).

The decomposition of $O_2^{\bullet-}$ was simulated assuming the pseudo-first-order rate law for the disproportionation reaction (see model and simulation details in SI). The shape of the i_T versus d curve depends strongly on the value of the effective rate constant (k_c). The fit in Figure 6b was obtained with k_c = 3.4×10^5 s^{-1}, which corresponds to the half-life of $O_2^{\bullet-}$ in aqueous solution, ln $2/k_c$ = 2 μs. To our knowledge, the lifetime of $O_2^{\bullet-}$ at a neutral pH has not yet been measured, and the only available literature data were obtained in alkaline solutions (e.g., at pH 10[40]).

Clearly, the determined k_c may be affected by the ORR-induced increase in solution pH near the substrate surface. This effect could be diminished in buffered solutions. However, the anions of common buffers (e.g., phosphate,[41] acetate,[42] and carbonate[43] species) are known to adsorb on Pt and influence the ORR kinetics. (For the same reason, we did not add Cl^- to aqueous solution and used Ag/AgCl as a quasi-reference electrode.) Moreover, a very high buffer concentration would be required to maintain essentially constant pH within the nanometer-thick layer of solution adjacent to the Pt surface.[44] The addition of concentrated buffer electrolyte to the aqueous phase would narrow the polarization window of the liquid/liquid interface and impair the measurement of the superoxide anion transfer. Therefore, we have chosen to carry out our experiments in sulfate solutions despite the possibility of underestimating k_c.

Another potential concern is a possibility of strong adsorption of TEA^+ on Pt and its effect on the ORR. While adsorption of TEA^+ on activated carbon[45a] and mercury[45b] has been reported, we were unable to find any literature evidence for specific adsorption of this species on Pt in the neutral aqueous solution. Ünlü et al.[45c] reported that quaternary ammonium cations can adsorb on Pt from strongly alkaline solutions and influence the kinetics of the oxidation of methanol.

The $O_2^{\bullet-}$ decomposition may be the fastest homogeneous kinetics measured electrochemically to date. The upper limit for the rate constant measurable by ET/IT SECM is determined by the attainable distance of the closest approach. The shortest separation distance in Figure 6b (~3 nm) is sufficiently small to measure the rate constants at least 2 orders of magnitude higher than the k_c value determined in this work. Unlike metal nanoelectrodes, a nanopipette used as an SECM tip can be brought extremely close to the conductive substrate surface (e.g., d = 1 nm[46]) without inducing electron tunneling. Thus, the developed approach is potentially promising for detecting charged intermediates of catalytic processes with the lifetime of a few nanoseconds.

CONCLUSIONS

Direct evidence of superoxide formation at the bare polycrystalline Pt surface during the ORR in neutral aqueous solution and its desorption has been obtained by using the SECM equipped with a nanopipette tip. The diffusion flux of superoxide at the electrode surface corresponds to about 9% fraction of reduced oxygen. The half-life of $O_2^{\bullet-}$ in aqueous solution was evaluated to be ~2 μs. The detection of superoxide radical in solution was possible because of the extremely high mass transfer rate of the SECM operated in the ET/IT mode. With the attainable distance of the closest approach between the nanopipette tip and catalytic substrate of about 1 nm, this technique should be capable of detecting ionic intermediates of heterogeneous reactions with the lifetime of a few nanoseconds.

IT voltammograms of the $O_2^{\bullet-}$ transfer across the liquid/liquid nanointerface were obtained for the first time. Ion transfer voltammetry can differentiate between the anionic, neutral, and cationic reaction intermediates because neutral molecules (e.g., $OH^{\bullet}$ or H_2O_2) do not contribute to the IT current, while positively and negatively charged transferred species produce the currents flowing in the opposite directions. The half-wave potential of the $O_2^{\bullet-}$ transfer was determined and used for unambiguous identification of this intermediate. This approach can be used for the detection and identification of charged intermediates of various heterogeneous chemical and electrochemical reactions in both aqueous and nonaqueous solutions.

ASSOCIATED CONTENT

Supporting Information

Characterization of nanopipettes, supplementary SECM data, mathematical model, and COMSOL simulation report. The Supporting Information is available free of charge on the ACS Publications website at DOI: 10.1021/ja512482n.

AUTHOR INFORMATION

Corresponding Author

*mmirkin@qc.cuny.edu

Notes

The authors declare no competing financial interest.

ACKNOWLEDGMENTS

The authors gratefully acknowledge support from the National Science Foundation (CHE-1416116), AFOSR MURI (FA9550-14-1-0003), and the Donors of the Petroleum Research Fund administrated by the American Chemical Society. We thank Allen Bard and Christian Amatore for valuable comments, Na Lei for preparing Figure 1, and Yixian Wang for her help with nanopipette silanization.

REFERENCES

(1) (a) Santos, E.; Schmickler, W. *Catalysis in Electrochemistry: From Fundamental Aspects to Strategies for Fuel Cell Development*; Wiley:

DOI: 10.1021/ja512482n
J. Am. Chem. Soc. 2015, 137, 6517−6523

Hoboken, NJ, 2011. (b) Jiao, Y.; Zheng, Y.; Jaroniec, M.; Qiao, S. Z. *Chem. Soc. Rev.* **2015**, *44*, 2060−2086.
(2) Markovic, N. M.; Schmidt, T. J.; Stamenkovic, V.; Ross, P. N. *Fuel Cells* **2001**, *1*, 105.
(3) Wu, J. B.; Yang, H. *Acc. Chem. Res.* **2013**, *46*, 1848.
(4) Xu, Y.; Shao, M.; Mavrikakis, M.; Adzic, R. R. Recent Developments in the Electrocatalysis of the O_2 Reduction Reaction. In *Fuel Cell Catalysis: A Surface Science Approach*; Koper, M. T. M., Ed.; Wiley: Hoboken, NJ, 2009; pp 271−315.
(5) Shao, M. H.; Liu, P.; Adzic, R. R. *J. Am. Chem. Soc.* **2006**, *128*, 7408.
(6) Hansen, H. A.; Viswanathan, V.; Norskov, J. K. *J. Phys. Chem. C* **2014**, *118*, 6706.
(7) Noel, J. M.; Latus, A.; Lagrost, C.; Volanschi, E.; Hapiot, P. *J. Am. Chem. Soc.* **2012**, *134*, 2835.
(8) Li, X.; Gewirth, A. A. *J. Am. Chem. Soc.* **2005**, *127*, 5252.
(9) Strbac, S.; Anastasijevic, N. A.; Adzic, R. R. *Electrochim. Acta* **1994**, *39*, 983.
(10) Postlethwaite, T. A.; Hutchison, J. E.; Murray, R.; Fosset, B.; Amatore, C. *Anal. Chem.* **1996**, *68*, 2951.
(11) Rodríguez-López, J.; Zoski, C. G.; Bard, A. J. SECM Applications to Electrocatalysis and Photocatalysis and Surface Interrogation. In *Scanning Electrochemical Microscopy*, 2nd ed.; Bard, A. J., Mirkin, M. V., Eds.; CRC Press: Boca Raton, FL, 2012; pp 525−568.
(12) Johnson, L.; Walsh, D. A. *J. Electroanal. Chem.* **2012**, *682*, 45.
(13) Liu, B.; Bard, A. J. *J. Phys. Chem. B* **2002**, *106*, 12801.
(14) Shen, Y.; Trauble, M.; Wittstock, G. *Anal. Chem.* **2008**, *80*, 750.
(15) Noel, J. M.; Yu, Y.; Mirkin, M. V. *Langmuir* **2013**, *29*, 1346.
(16) Yang, H. H.; McCreery, R. L. *J. Electrochem. Soc.* **2000**, *147*, 3420.
(17) Zhang, C.; Fan, F. R.; Bard, A. J. *J. Am. Chem. Soc.* **2009**, *131*, 177.
(18) Wang, Y. X.; Kececi, K.; Velmurugan, J.; Mirkin, M. V. *Chem. Sci.* **2013**, *4*, 3606.
(19) Girault, H. H. Electrochemistry at Liquid−Liquid Interfaces. In *Electroanalytical Chemistry*; Bard, A. J., Zoski, C. G., Eds.; CRC Press: Boca Raton, FL, 2010; pp 1−104.
(20) Yatziv, Y.; Turyan, I.; Mandler, D. *J. Am. Chem. Soc.* **2002**, *124*, 5618.
(21) Lin, C. L.; Rodriguez-Lopez, J.; Bard, A. J. *Anal. Chem.* **2009**, *81*, 8868.
(22) Olaya, A. J.; Ge, P. Y.; Girault, H. H. *Electrochem. Commun.* **2012**, *19*, 101.
(23) Ohrenberg, C.; Geiger, W. E. *Inorg. Chem.* **2000**, *39*, 2948.
(24) Clarke, D. J.; Schiffrin, D. J.; Wiles, M. C. *Electrochim. Acta* **1989**, *34*, 767.
(25) Shao, Y. H.; Mirkin, M. V. *J. Am. Chem. Soc.* **1997**, *119*, 8103.
(26) Wang, Y. X.; Velmurugan, J.; Mirkin, M. V.; Rodgers, P. J.; Kim, J.; Amemiya, S. *Anal. Chem.* **2010**, *82*, 77.
(27) Kim, J.; Shen, M.; Nioradze, N.; Amemiya, S. *Anal. Chem.* **2012**, *84*, 3489.
(28) Nogala, W.; Velmurugan, J.; Mirkin, M. V. *Anal. Chem.* **2012**, *84*, 5192.
(29) Sawyer, D. T.; Valentine, J. S. *Acc. Chem. Res.* **1981**, *14*, 393.
(30) Andrieux, C. P.; Hapiot, P.; Saveant, J. M. *J. Am. Chem. Soc.* **1987**, *109*, 3768.
(31) Roberts, J. L.; Calderwood, T. S.; Sawyer, D. T. *J. Am. Chem. Soc.* **1983**, *105*, 7691.
(32) Zhang, M. A.; Chen, C. C.; Ma, W. H.; Zhao, J. C. *Angew. Chem., Int. Ed.* **2008**, *47*, 9730.
(33) Cornut, R.; Lefrou, C. *J. Electroanal. Chem.* **2007**, *608*, 59.
(34) Rodgers, P. J.; Amemiya, S. *Anal. Chem.* **2007**, *79*, 9276.
(35) Sawyer, D. T.; Chlericato, G.; Angelis, C. T.; Nanni, E. J.; Tsuchiya, T. *Anal. Chem.* **1982**, *54*, 1720.
(36) Lange, N. A.; Dean, J. A. *Lange's Handbook of Chemistry*, 13th ed.; McGraw-Hill Press: New York, 1985; pp 5−15.
(37) Bard, A. J.; Faulkner, L. R. *Electrochemical Methods: Fundamentals and Applications*; Wiley: Hoboken, NJ, 2000.
(38) Okuda, M.; Tsuruta, T.; Katayama, K. *Phys. Chem. Chem. Phys.* **2009**, *11*, 2287.
(39) The i_{max} value was evaluated using the Dc^* value extracted from steady-state voltammograms of the one-electron ORR in BTF. The ratio of oxygen diffusion coefficients in water and BTF was estimated using the Walden rule and BTF and water viscosity values of 0.55 and 0.97 mPa·s, respectively (Viswanath, D. S.; Ghosh, T.; Prasad, D. H. L.; Dutt, N. V. K.; Rani, K. Y. *Viscosity of Liquids: Theory, Estimation, Experiment, and Data*; Springer: New York, 2007).
(40) Zang, L. Y.; Misra, H. P. *J. Biol. Chem.* **1992**, *267*, 23601.
(41) (a) Gisbert, R.; García, G.; Koper, M. T. M. *Electrochim. Acta* **2010**, *55*, 7961. (b) He, Q.; Yang, X.; Chen, W.; Mukerjee, S.; Koel, B.; Chen, S. *Phys. Chem. Chem. Phys.* **2010**, *12*, 12544.
(42) Fukuda, T.; Aramata, A. *J. Electroanal. Chem.* **1999**, *467*, 112.
(43) Iwasita, T.; Rodes, A.; Pastor, E. *J. Electroanal. Chem.* **1995**, *383*, 181.
(44) Horrocks, B. R.; Mirkin, M. V.; Pierce, D. T.; Bard, A. J.; Nagy, G.; Toth, K. *Anal. Chem.* **1993**, *65*, 1213.
(45) (a) Tamai, H.; Kunihiro, M.; Yasuda, H. *J. Colloid Interface Sci.* **2004**, *275*, 44. (b) Devanathan, M. A. V.; Fernando, M. J. *Trans. Faraday Soc.* **1962**, *58*, 368. (c) Ünlü, M.; Abbott, D.; Ramaswamy, N.; Ren, X.; Mukerjee, S.; Kohl, P. A. *J. Electrochem. Soc.* **2011**, *158*, B1423.
(46) Elsamadisi, P.; Wang, Y. X.; Velmurugan, J.; Mirkin, M. V. *Anal. Chem.* **2011**, *83*, 671.

DOI: 10.1021/ja512482n
J. Am. Chem. Soc. 2015, 137, 6517−6523